



Pulsed potential co-electrodeposition of $\text{Cu}_2\text{CoSnS}_4$ absorber layer on fluorinated tin oxide (FTO)-coated glass

Omar Ait Layachi¹ · Abderrazzak Boudouma¹ · Mohammed Lasri² · Hala Hrir¹ · Meryem Nini¹ · Sara Azmi³ · Mohammed Bousseta⁴ · Asmaa Moujib¹ · El mati Khoumri¹

Received: 31 January 2024 / Accepted: 20 April 2024
© The Author(s), under exclusive licence to Springer Nature B.V. 2024

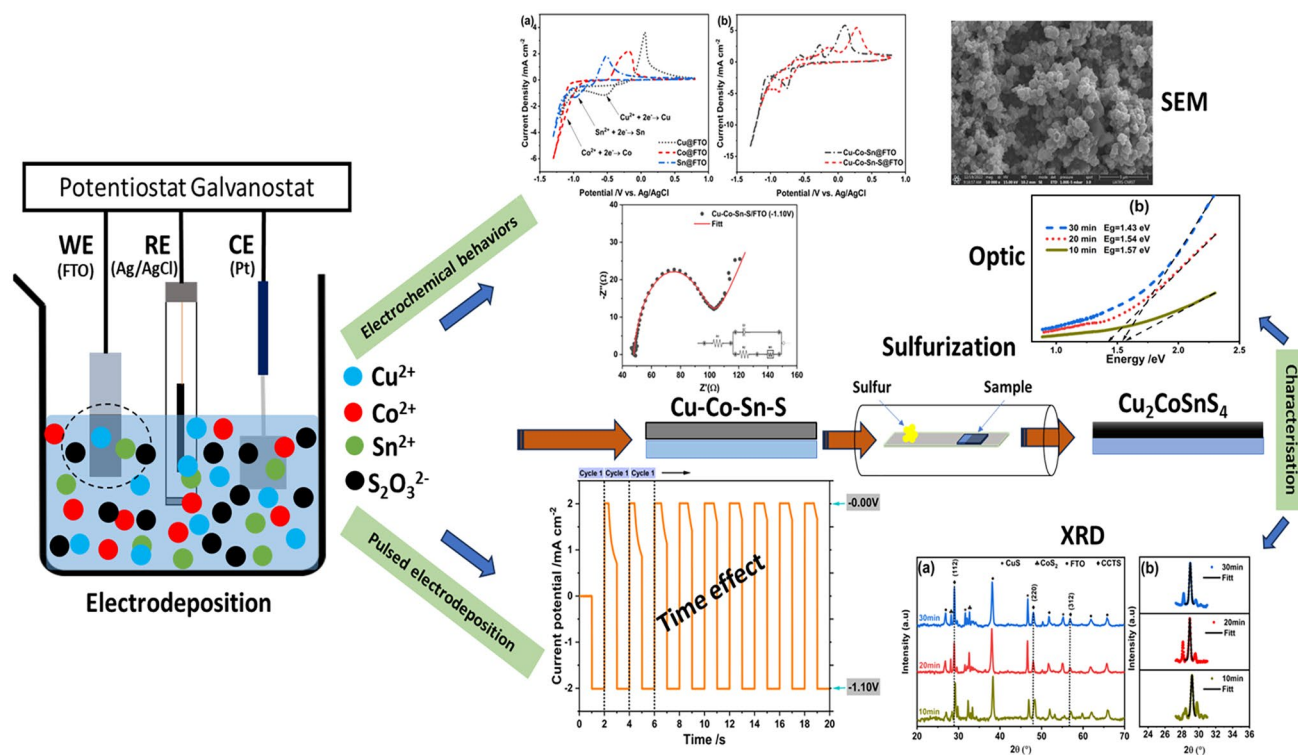
Abstract

Thin films of $\text{Cu}_2\text{CoSnS}_4$ (CCTS) are electrodeposited onto fluorine tin oxide substrate using pulsed electrodeposition mode for various time periods followed by sulfurization treatment at 500 °C. The pulse potential (V1) is held constant at 0 V vs. Ag/AgCl, while (V2) is set at - 1.1 V vs. Ag/AgCl. The effect of pulse duration on the CCTS propriety is being investigated. Cyclic voltammetry was used to study the electrochemical behaviors of Cu–Co–Sn–S precursors, while in situ electrochemical impedance spectroscopy investigated the electrical properties of the system during electrodeposition of CCTS at - 1.10 V. The impedance spectra revealed a capacitive loop pattern along with Warburg diffusion. The samples were analyzed by X-ray diffraction (XRD), Raman spectroscopy, and UV–visible spectroscopy. Both XRD data and Raman spectra indicated that the CCTS thin films have a stannite structure. The films deposited for 20 min and 30 min exhibit a predominantly pure CCTS phase. Moreover, deposition for 20 min exhibits a homogeneous morphology with a nearly stoichiometric composition along with an optical band gap energy of 1.54 eV. Apart from the CCTS phase, noticeable secondary phases are present in films deposited at both low and high pulse durations, and they have been observed to slightly affect the gap energy.

✉ Omar Ait Layachi
aitlayachiomar@gmail.com;
omar.aitlayachi-etu@etu.univh2c.ma

- ¹ Laboratory of Physical Chemistry and Biotechnology of Biomolecules and Materials, Faculty of Sciences and Technology, Hassan II University of Casablanca, 20650 Mohammedia, Morocco
- ² Laboratory of Applied Chemistry and Biomass, Department of Chemistry, Faculty of Sciences, University Cadi Ayyad, Semlalia, BP 2390, Marrakech, Morocco
- ³ Laboratory of Mechanics and Civil Engineering (LMGC), CNRS, University of Montpellier, 34090 Montpellier, France
- ⁴ Laboratory of Materials, Energy, and the Environment (LaMEE), Faculty of Science Semlalia, Cadi Ayyad University, P. O. Box 2390, 40000 Marrakech, Morocco

Graphical abstract



Keywords $\text{Cu}_2\text{CoSnS}_4$ · Stannite · Pulsed electrodeposition · Time effect · Thin film · Solar cells

1 Introduction

Extensive research efforts have focused on quaternary chalcogenide materials. This surge in interest is due to the remarkable electronic and electrical properties of these compounds. These properties make them highly promising for applications in photonic devices [1]. Recently, a conversion efficiency of 14.9% has been achieved with the readily available solar absorber $\text{Cu}_2\text{ZnSnS}_4(\text{Se})$ [2], known for its high absorption coefficient (above 10^4 cm). $\text{Cu}_2\text{CoSnS}_4$ (CCTS) belongs to the chalcopyrite family of inorganic semiconductors and offers a comparable and viable alternative absorbing material. CCTS crystallizing in quadratic system (I4m group) [3] and has an ideal bandgap in the range of 1.2–1.5 eV making it exceptionally well suited for various photonic applications. This optimal bandgap range positions CCTS as a promising candidate for harnessing solar energy and advancing photovoltaic technology [4–7]. Its potential for integration into next-generation optoelectronic devices is further enhanced by its structural and electronic properties.

Several synthetic techniques, such as, sputtering [8], pulsed laser deposition [9], microwave method [10], thermal decomposition [11], chemical vapor deposition [12],

spray pyrolysis [13, 14], solid-state reaction [15], colloidal synthesis [16], and electrochemical deposition (electrodeposition) [17–20], have been used to fabricate CCTS thin films. Among these approaches, electrochemical deposition stands out as a highly attractive method. This is due to its advantages, including economical equipment, inexpensive starting materials, and the ability to perform scalable deposition at room temperature. Some research has been conducted to investigate the factors that affect the electrochemical deposition process for the preparation of CCTS. Electrodeposition techniques include sequential deposition of metallic stacked Cu, Zn, and Sn thin films followed by sulfur (S) diffusion, simultaneous deposition of metallic Cu, Zn, and Sn thin films followed by sulfur (S) diffusion, and single-step deposition of CZTS thin film has been reported in several studies. Pulsed electrodeposition technique (PED) has found wide application in metal plating, effectively increasing deposition rates and refining film quality [21]. PED has been used in CZTS deposition to improve film quality [22–24]. However, its use in the growth of CCTS thin films has not been explored. PED differs from conventional DC electrodeposition primarily in the controlled on/off cycling of the plating currents.

This results in the generation of a square wave pattern that is characterized by specific pulse parameters, including pulse duration (T_{ON}), time between pulses (T_{OFF}), and the overall deposition duty cycle. Pulsed Electrodeposition (PED) provides the flexibility to create complex alloy compositions. By precisely adjusting metal ion concentrations, current densities and pulse durations, the formation of new crystals can be stimulated rather than the growth of existing ones. The result is the production of films with an exceptionally fine grain structure [25].

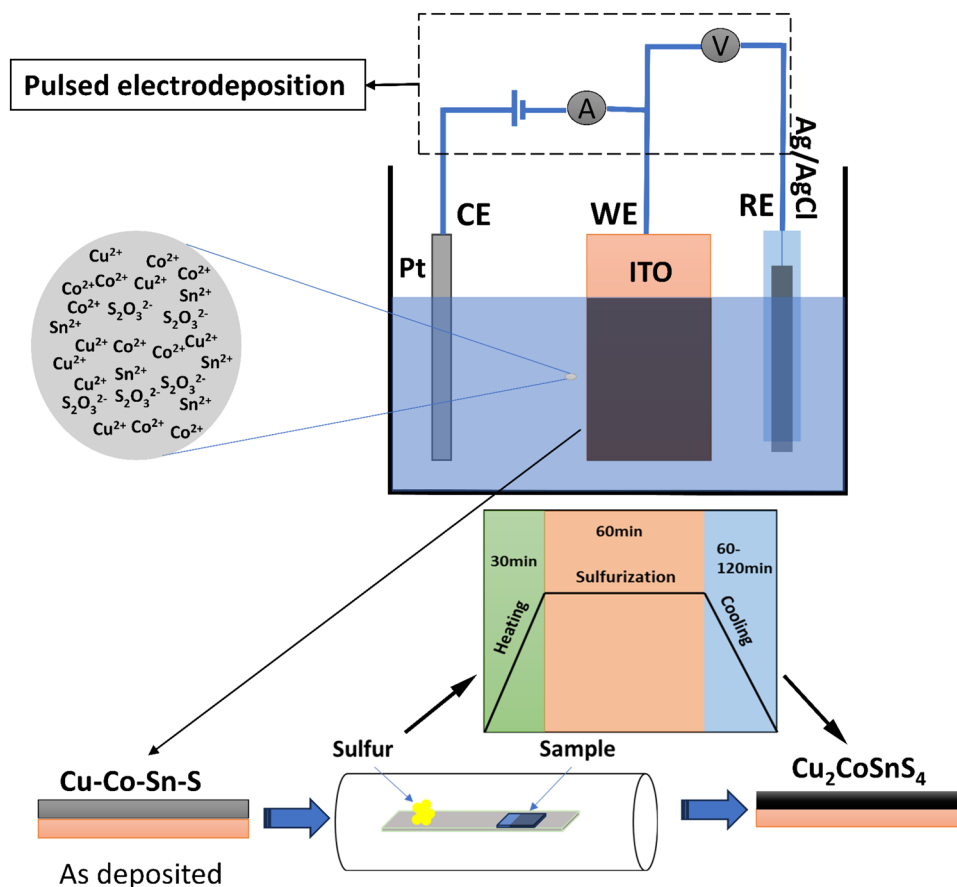
2 Experimental

The pulse electrodeposition (PED) process was performed using a standard three-electrode potentiostat (VersaSTAT 3). Fluorine tin oxide (FTO) was employed as a working electrode, a Platine electrode was used as the counter electrode, while Ag/AgCl/ Cl^- was used as the reference electrode (Fig. 1). The aqueous electrolytic solution consists of $CuSO_4 \cdot 5H_2O$ (0.02 M), $CoCl_2 \cdot 6H_2O$ (0.015 M), $SnSO_4$ (0.010 M) and $Na_2S_2O_3$ (0.02 M), with $Na_3C_6H_5O_7 \cdot 2H_2O$ (0.2 M) acting as a complex agent. The

pH of the solution was adjusted to 5.0 by the addition of an appropriate amount of tartaric acid. The CCTS thin films were prepared by potentiostatic electrodeposition using potential-pulsed electrodeposition at -1.1 V with a pulse duration of 1 s and an off-time (0 V) of 1 s (Fig. 2c). The total electrodeposition time was 10 min (CCTS1), 20 min (CCTS2), and 30 min (CCTS3). The Cu–Co–Sn–S electrodeposited precursor films were sulfurized by exposure to an evaporated sulfur environment at $T = 500$ °C for 1 h in an alumina tube furnace, resulting in the formation of CCTS films. To eliminate any trace of air, the tube was purged with Ar gas for 15 min prior to sulfurization. 0.8 g sulfur (with a purity of 99.9%) was used as the source and was placed in an alumina boat that was maintained at a temperature of 25 °C.

The sulfurized thin films were structurally analyzed using X-ray diffraction (XRD) with $CuK\alpha$ radiation ($\lambda = 1.5406$ Å). A field emission scanning electron microscope (FE-SEM) (model) and an energy dispersive X-ray spectrometer (EDS) were used for surface morphological and compositional characterization. UV–visible–NIR spectroscopy (SHIMADZU, UV-2600i) was used to measure the optical properties of the thin films at room temperature.

Fig. 1 Schematic of synthesis of CCTS thin films



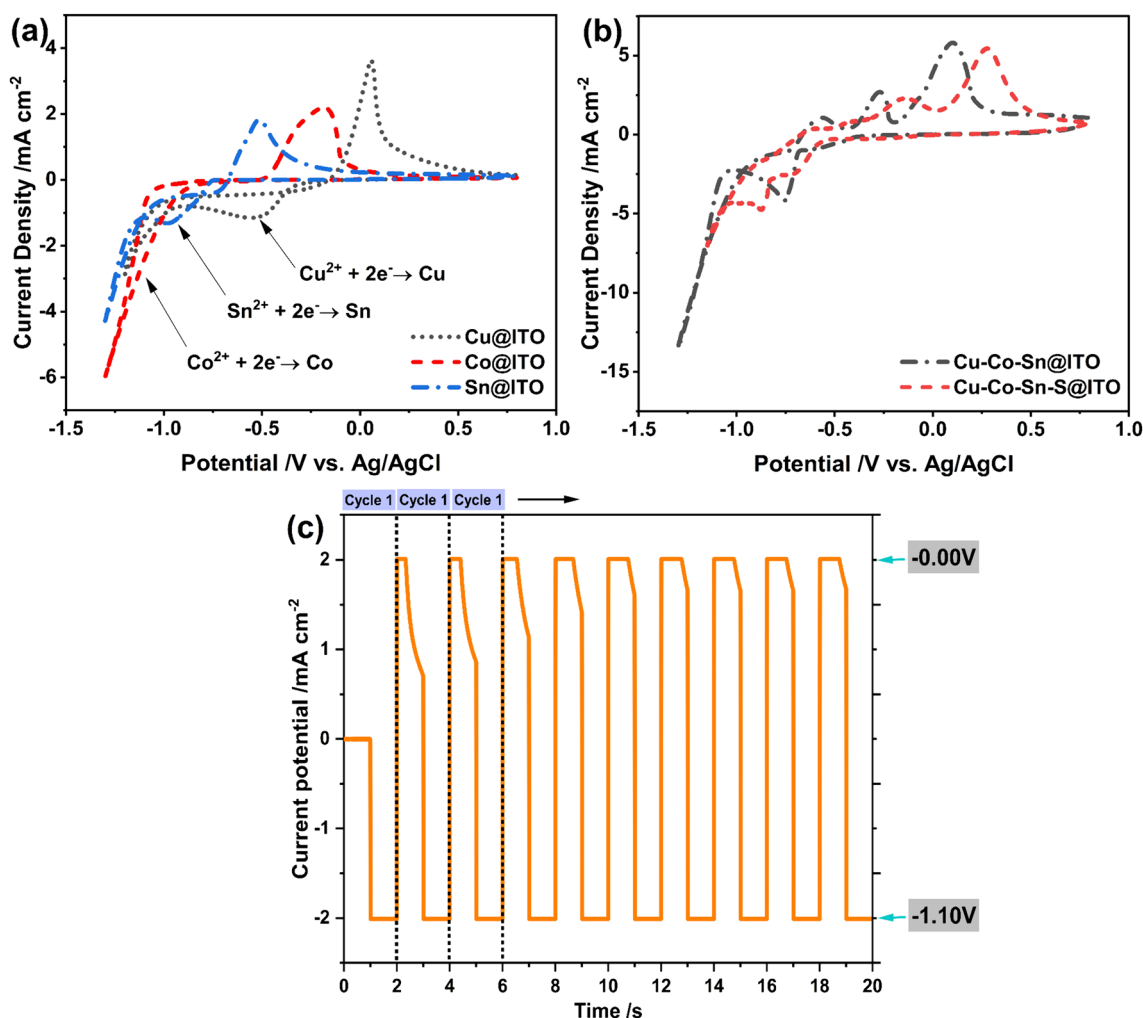


Fig. 2 **a** Cyclic voltammograms in trisodium citrate solution for each individual element: Cu²⁺, Co²⁺, and Sn²⁺. **b** Cyclic voltammetry in trisodium citrate solution for combined elements: Cu²⁺-Co²⁺-Sn²⁺-

S²⁻. **c** Current density/mA cm⁻² vs. time/s in pulsed electrodeposition [$E_1 = 0.00$ V, $E_2 = -1.10$ V vs. Ag/AgCl]

3 Results and discussion

3.1 Electrochemical characterization

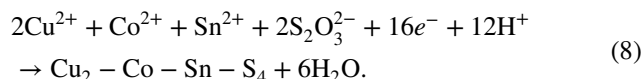
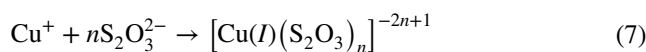
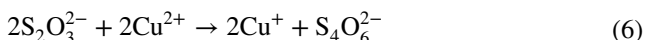
Cyclic Voltammetry (CV) is a valuable technique providing insights into the reduction potential of elements within the electrolytic bath, crucial for understanding the electrochemical behavior and reactivity of the deposition process components. To determine the deposition potential of the CCTS precursor, the individual deposition potentials of copper (Cu), cobalt (Co), and tin (Sn) were first determined using separate electrolytic baths. Subsequently, the deposition potential of CCTS films was thoroughly evaluated for the influence of complexing agents and thiosulfate elements (S₂O₃²⁻). This comprehensive approach ensured a detailed understanding of the factors influencing the deposition process. The electrochemical behaviors of each element in the

aqueous solution reveal significant potential differences for Cu, Co, and Sn [26].

To refine the potential window, trisodium citrate was used as a complexing agent in the electrolytic bath. This compound forms complexes with copper ions (Cu²⁺), effectively shifting the reduction potential of copper to more negative values. A more controlled deposition process was achieved by this adjustment [26, 27].

Figure 2a depicts the electrochemical behavior of each individual element: Cu²⁺, Co²⁺, and Sn²⁺. The curves display cathodic and anodic peaks observed between -1.3 and 0.8 V vs. Ag/AgCl. The cathodic peaks of Cu²⁺, Sn²⁺, and Co²⁺ are located around -0.56 V, -0.98 V, and -1.10 V vs. Ag/AgCl, respectively. Figure 2b presents the cyclic voltammetry (CV) curve of the co-electrodeposition bath containing Cu²⁺, Sn²⁺ and Co²⁺. The voltammogram showed three distinct peaks. These peaks were consistent with the curves of the individual

metallic elements shown in Fig. 2a (Eqs. 1, 2, 3). This observation is an indication that the formulation was well suited for the deposition of Cu–Co–Sn films (Fig. 2b) [18, 27]. Additionally, these elements can be deposited with sulfur in the presence of $S_2O_3^{2-}$ which can generate colloidal S in acidic medium (Eqs. 4, 5) (Fig. 2b) [28]. $S_2O_3^{2-}$ could be introduced as a complexing agent for Cu^{2+} , as described by (Eqs. 6, 7) [29]. The overall electrodeposition reaction of Cu–Co–Sn–S precursors is represented by (Eq. 8).



The deposition of CCTS films was carried out using pulsed electrodeposition for durations of 10, 20, and 30 min. This involved applying a high potential (On; -1.1 V) in a series of pulses separated by intervals of 1 s with no potential flow (Off; 0 V) (Fig. 2c) [24].

Electrochemical impedance spectroscopy (EIS) was investigated to evaluate the behaviors of the electrochemical process associated with CCTS electrodeposition. The EIS were performed at both the potential of deposition (-1.10 V) and at the potential of (0.00 V). In Fig. 3 the dotted curves shows the experimental Nyquist diagrams in different situations, while the solid line represents the fit of the respective nyquist spectra.

The nyquist plot in Fig. 3a shows an in-situ impedimetric spectra at applied potential of $E=0.00$ V tilted by an angle θ to the y-axis. This implies that the equivalent circuit comprises either a standalone capacitor C which represents the nonfaradaic current results from charging the double-layer capacitor [30] or a capacitor C connected in

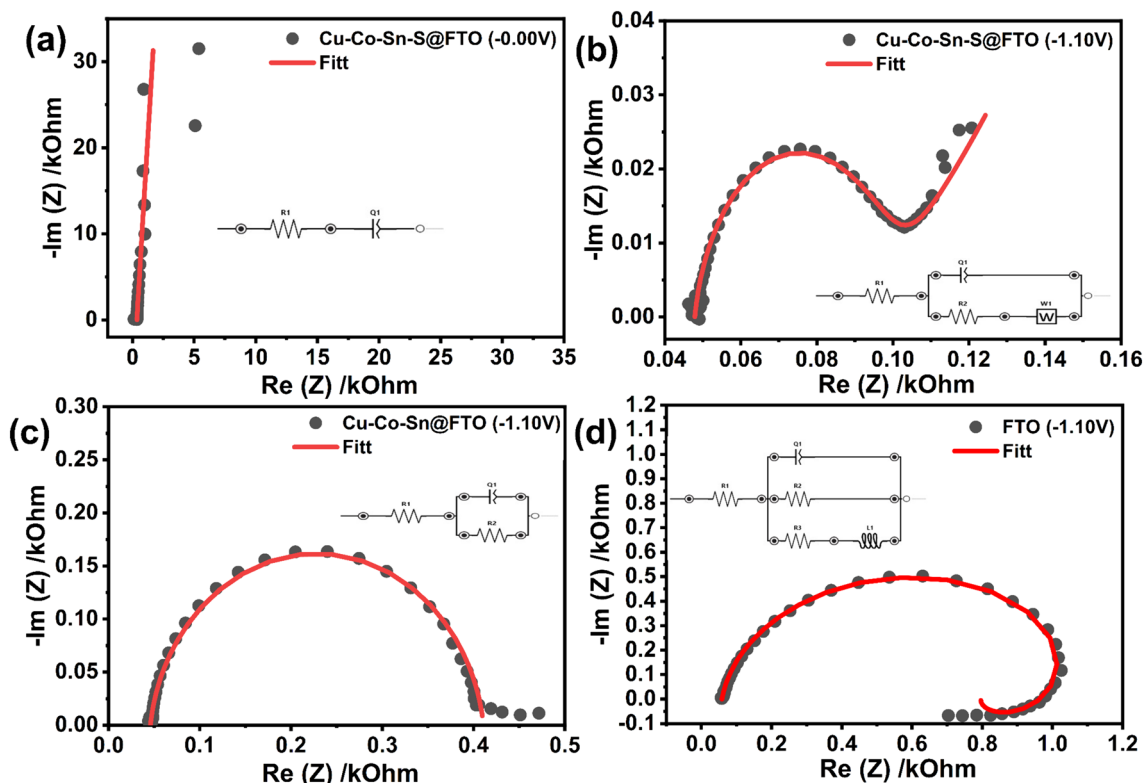
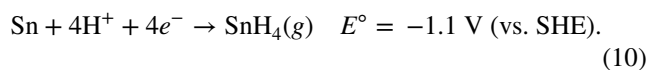
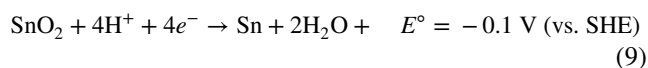


Fig. 3 In-situ electrochemical impedance spectroscopy measurements: **a** CCTS precursor deposition at 0.00 V, **b** CCTS precursor deposition at -1.1 V, **c** CCT precursor deposition at -1.1 V and **d** without electroactive species at -1.1 V

series with a solution resistor R_s [31]. The circuit fitting (Fig. 3a) suggests that the impedance is not purely ohmic and includes a capacitive element (CPE) [30]. This could be due to surface effects, double-layer capacitance, or other non-idealities [32]. In another hand, the EIS spectra recored at $E = -1.10$ V a semicircle at high and medium frequency is related to the double layer response and an inclined line at low frequency indicated the presence of a warburg impedance due to diffusion of ions into the electrode surface. The impedance plotted in Fig. 3b was fit to the equivalent circuit shown in the same figure. This circuit consists of a parallel combination of a series charge transfer resistance (R_{ct}) and a Warburg element (W), along with a constant phase element (CPE) representing the double-layer capacitance [33, 34]. In addition, the solution resistance is represented by the series resistance (R_s). The fitted lines in Fig. 3b correspond to this equivalent circuit [34]. The values for the various elements are given in Table 1. The effective double-layer capacitance, Q , was determined from the constant phase element using a method explained by Mansfeld [35, 36]. Figure 3c presented the impedance spectra conducted in situ during electrodeposition of Cu–Co–Sn in a free sulfur solution. The results shows the presence of a capacitive loop without Warburg impedance. This may mean that charge transfer at the electrode/electrolyte interface is relatively fast and mass transport limitations (typically represented by Warburg impedance) are not significant during the electrodeposition process. Additionally, The absence of a Warburg impedance may indicate that the electrodeposited layer is relatively thin. The difference in the impedance spectra between Fig. 3b and c can demonstrate the interaction between $S_2O_3^{2-}$ and metal ions in the electrodeposition process, as indicated by Eqs. (2) and (3). Furthermore, the electrochemical impedance behaviors of FTO electrode in the citrate electrolyte at the same potential (-1.10 V) and in absence of the electroactive elements was studied. Figure 3d presents the impedance spectra obtained by the experiment. It reveals the presence of high-frequency capacitive loop, associated with double layer capacitance, and the appearance of inductive loop representing the relaxation phenomena. This relaxation is likely dependent of the presence of $(Sn(IV))_{ads} \equiv (SnH_4)_g$ as an adsorbed intermediate species in the reduction reaction tin oxyde (comprising 95% FTO [37]) [34]. This reduction reactions denoted by Eqs. (9) and (10) is induced by cathodic polarisation on the surface of the FTO electrode [38, 39].



3.2 Structural characterization

The precursor electrodeposited samples of CCTS were sulfurized at a temperature of 500 °C for one hour in the presence of sulfur powder.

3.2.1 XRD analysis

Figure 4a shows the XRD patterns of CCTS films obtained by pulsed electrodeposition of Cu–Co–Sn–S precursor films at 10, 20 and 30 min. All the films aligned with the tetragonal structure of CCTS, as indicated by the four distinctive peaks (112), (204), and (312) observed at 2θ values of 28.90° , 47.92° , and 56.72° , respectively, in accordance with JCPDS 96-153-3608. The secondary phases produced in all cases is CoS_2 at 32.5° (card no. 00-041-1471) [40]. Additionally, the peak observed around 31.6° in samples electrodeposited for 20 and 30 min indicates the presence of CuS (card no. 00-006-0464) [41]. The other peaks located at 26.9° , 38.1° , 51.74° , 61.7° , and 65.7° are associated with the FTO substrate [27, 28, 42]. Using the Gaussian fitting (Fig. 4b), the average crystallite sizes of the CCTS films were determined by calculating the full width at half maximum (FWHM) of the peak through the application of the Debye–Scherrer equation. The CCTS film crystallite sizes

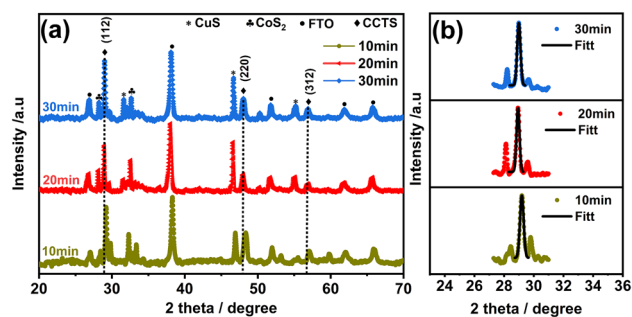


Fig. 4 X-ray diffraction analysis of CCTS thin films for various pulse durations

Table 1 Simulated impedance parameters

Element	R_1/Ohm	Q_1/mF	n_1	R_2/Ohm	$W_1/\text{Ohm s}^{-0.5}$	R_3/Ohm	L_1/H
(a)	254.7	3.204	0.934	–	–	–	–
(b)	47.90	0.276	0.883	50.92	20.67	–	–
(c)	45.95	43.76	0.927	363.90	–	–	–
(d)	58.48	10.22	0.919	1170.00	–	1999.00	70.00

resulting from electrodeposition of CCTS precursor films at duty 10 min, 20 min and 30 min were 28.36.6 nm, 27 nm, and 24 nm, respectively (Table 2). According to the observations mentioned earlier, an increase in deposition time led to a minor reduction in crystallite sizes, aligning well with the findings from scanning electron microscopy (SEM) (Fig. 6).

3.2.2 Raman analysis

Figure 5 shows the Raman spectra (200–600 cm^{-1}) of the CCTS samples deposited for different time periods. The spectra obtained showed a principal sharp peak at 470 cm^{-1} consistently in all cases, along with a less prominent peak at 265 cm^{-1} . Both peaks are characteristic of a crystalline structure, indicating a single crystal of CuS [43]. The several peaks located at 280–290 cm^{-1} and 318–334 cm^{-1} correspond to the $\text{Cu}_2\text{CoSnS}_4$ phase. The most prominent peak occurs in the range of 318–319 cm^{-1} and is associated with the A1 symmetry of the CCTS stannite structure. The peak located at 490 cm^{-1} in 30 min sample may indicate the presence of CoS phase [44]. As a result, the samples electrodeposited for 20 and 30 min confirm the presence of a pure CCTS phase.

3.3 Morphological characterization

Figure 6a–c, shows SEM images of CCTS pulsed electrodeposited thin films on the FTO substrate at different deposition time. The sample deposited for 10 min shows a uniform morphology (Fig. 6a), but as the deposition time increases to 20 min (Fig. 6b), a decrease in grain size is observed. This phenomenon can be attributed to increased nucleation leading to the formation of a wider number of smaller grains. On the other hand, prolonging the deposition time to 30 min through pulsed electrodeposition (Fig. 6c) results in smaller grain sizes. Simultaneously, an additional morphology with a hexagonal sheet-like structure appears, possibly associated with the secondary phase CuS [45].

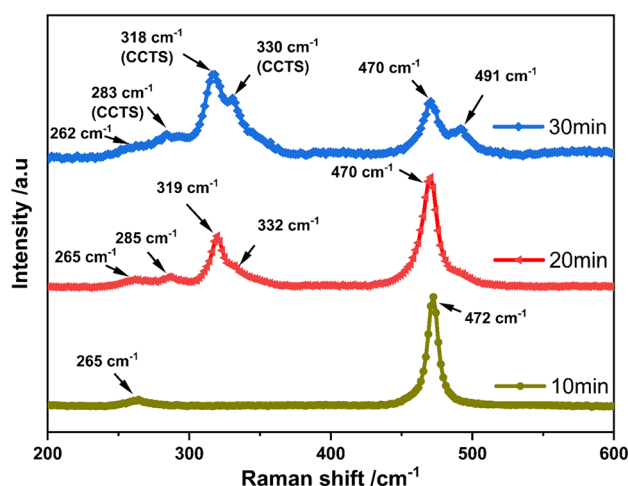


Fig. 5 Raman spectra analysis of CCTS samples

Quantitative EDS analysis was performed on thin films electrodeposited for 10, 20, and 30 min. Figure 7 shows an EDS spectrum showing the presence of different peaks associated with Cu, Co, Sn and S, corresponding to the deposited CCTS thin film. In addition, the presence of an O peak originating from the FTO substrates was observed. The atomic composition (Table 3) indicates the sulfur-rich nature of the films. The presence of Cu is likely contributed by the CuS phases, and the 10 min sample shows Sn-rich grains, possibly due to its association with one of the FTO compositions. The ratio ($\text{Cu}/(\text{Co} + \text{Sn})$) decreases, reaching approximately 1 as the deposition time increases. The proportion of Co increases while the amount of Sn decreases. The ratio ($\text{Cu}/(\text{Co} + \text{Sn})$) decreases, reaching approximately 1 as the deposition time increases (Table 3).

3.4 Optical characterization

The UV–Vis absorption spectra of the CCTS electrodeposited samples are shown in Fig. 8a. These spectra were

Table 2 Structural parameters of CCTS thin films

Deposition time	(hkl)	2Theta/ $^\circ$	FWHM/ $^\circ$	D /nm	d-spacing/ \AA	a/ \AA	c/ \AA
10 min	112	29.195	0.27	31.3	3.056	5.367	10.309
	204	46.929	0.264	33.9	1.934		
	312	57.08	0.469	19.9	1.612		
20 min	112	28.942	0.221	38.5	3.082	5.374	10.540
	204	48.005	0.392	22.6	1.893		
	312	56.876	0.461	19.9	1.617		
30 min	112	28.995	0.255	33.2	3.077	5.376	10.478
	204	48.039	0.443	20	1.892		
	312	56.89	0.489	18.8	1.617		

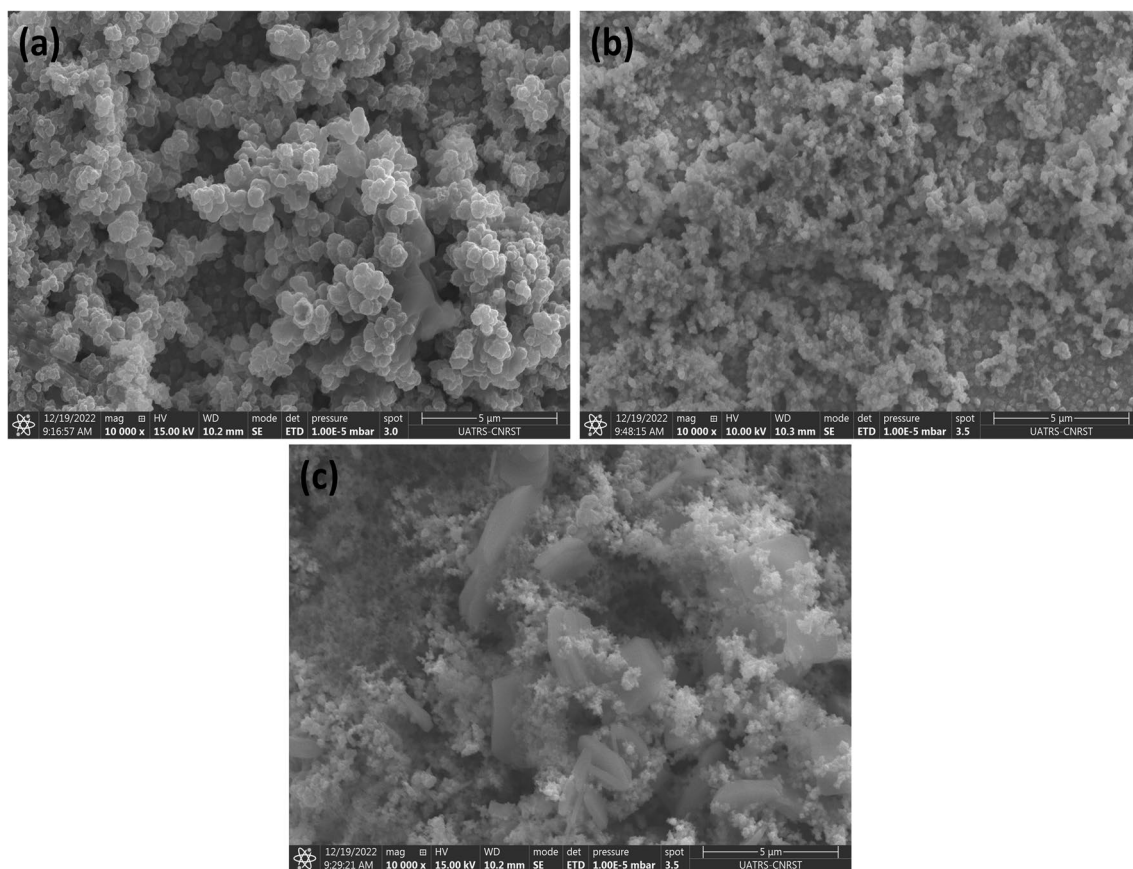


Fig. 6 SEM-images of CCTS thin films; electrodeposited for: **a** 10 min, **b** 20 min and **c** 30 min

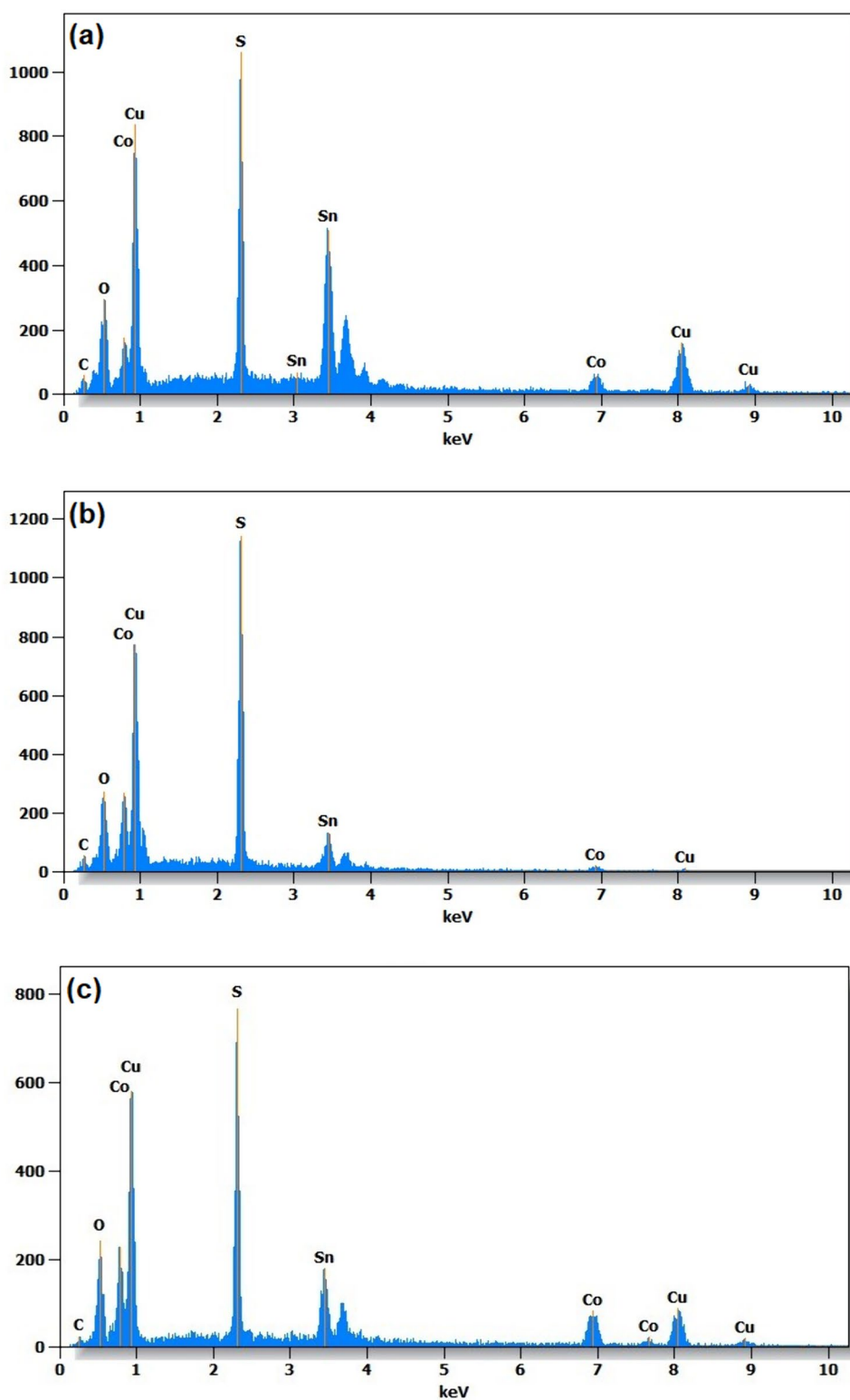
measured in the absorbance mode over the wavelength range of 400–1200 nm. The absorption spectra show a decrease in intensity with increasing deposition time. This is likely due to an increase in thickness uniformity of the film as the deposition time increases. The straight-line segments of the Tauc's plots shown in Fig. 8b are extended to the point where the absorption coefficient reaches zero, providing intercepts or values for the band gap. The band gap values for the 10 min, 20 min, and 30 min films are 1.57 eV, 1.54 eV, and 1.43 eV, respectively. The band gap (E_g) values show a slight decrease over time, increasing by 0.03 eV from CCTS 10 min to CCTS 20 min, and by 0.11 eV from CCTS 20 min to CCTS 30 min. This change is attributed to variations in structural composition and morphology [46], as illustrated in Figs. 5, 6, and Table 3. Despite the slight impact of deposition time on the E_g values of CCTS thin films due to the presence of secondary phases [18], all films have a band gap aligned with the optimum energy range for thin film solar cells, making them suitable for applications in thin film solar cells with high conversion efficiency. This value is consistent with

those reported in the literature [14, 47]. Table 4 presents a comparative analysis of CCTS thin films elaborated by co-electrodeposition and our study, which investigated pulsed mode electrodeposition.

4 Conclusion

In this study, we present an economical approach for manufacturing CCTS thin films on an FTO-coated glass surface. The pulsed electrodeposition method (PED), followed by a sulfurization treatment at 500 °C in argon atmosphere, proved successful in the fabrication of CCTS films. The crucial parameter in pulsed electrodeposition (PED) is the pulse duration with predefined potentials. The electrochemical behaviors of CCTS precursors have been studied individually using cyclic voltammetry, as well as together in the same bath containing trisodium citrate. In-situ electrochemical impedance spectroscopy (EIS) has investigated the mechanism of deposition at the electrode–electrolyte interface. The impedance spectra reveal a loop capacitive behavior, and in the presence of

Fig. 7 EDS analysis of CCTS thin films; **a** 10 min, **b** 20 min and **c** 30 min

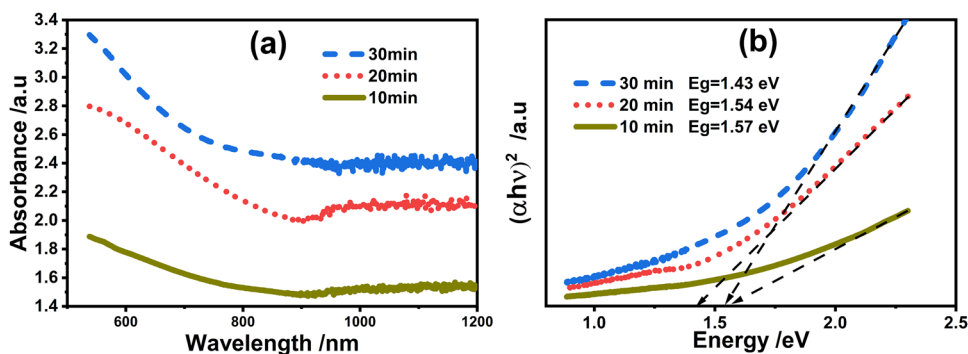


$S_2O_3^{2-}$, they indicate the presence of Warburg diffusion, suggesting a diffusion phenomenon. CCTS deposited for 20 min exhibited a pure CCTS phase, compact morphology, and nearly stoichiometric composition. Conversely,

pulsed electrodeposition of CCTS for 10 min revealed the presence of secondary phases. The optical gap energy is slightly affected by the deposition time and was found to be around 1.50 eV, making it well-suited for utilization

Table 3 Elemental composition of CCTS thin films

	Cu (%)	Co (%)	Sn (%)	S (%)	[Cu]/([Co] + [Sn])	[Co]/[Sn]	S/metal
10 min	19.1	3.6	10.1	51.2	1.39	0.35	1.56
20 min	18.0	5.4	6.0	45.3	1.57	0.9	1.54
30 min	17.3	9.9	5.5	50.1	1.12	1.8	1.53

Fig. 8 **a** UV–visible absorption measurements, **b** Tauc plots of CCTS thin films electrodeposition**Table 4** Comparative analysis of CCTS electrodeposition results

Mode electrodeposition	Electrolyte	Deposition conditions	Substrate	Important results	References
Co-electrodeposition	Tartaric acid, pH 4.8	Ed = − 0.850, − 0.90 and − 0.950 V (vs SCE) for 20 min Sulfurization: 500 °C	FTO	As the (Ed) increases from − 850 to − 950 mV, the optical gap expands from 1.50 to 1.60 eV	[17]
Co-electrodeposition	Tartaric acid Trisodium citrate, pH 4–5	Ed = − 0.95 V (vs SCE) for 15 min Sulfurization: 500 °C for 60 min	Mo	Tetragonal structure, gap energy = 1.56 eV	[18]
Co-electrodeposition	Trisodium citrate, pH 4–5	Ed = − 0.95 V (vs. SCE) for 15 min, 30 min and 45 min, Sulfurization: 500 °C for 60 min	Mo	Stannite structure Eg = 1.4–1.5 eV, slightly influenced by deposition time	[48]
Co-electrodeposition	Tartaric acid, pH 5	Ed = − 0.9 V vs. (SCE). Deposition time: 20 min. Sulfurization: 500 °C	Mo	The CCTS optical gap reduces from 1.68 to 1.48 eV when copper concentrations increase from 0.015 to 0.030 M	[49]
Co-electrodeposition	Trisodium citrate, (additive effects), pH 5	Ed = − 1.1 V vs. Ag/AgCl. Deposition time = 10 min. Sulfurization: 550 °C	FTO	Stannite structure. Additives influenced the CCTS properties Gap energy = 1.5 eV	[50]
Pulsed electrodeposition	Trisodium citrate, pH 5	Eon = − 1.1 V vs. Ag/AgCl (On) Eoff = 0 V Deposition time: 10, 20, and 30 min Sulfurization: 500 °C	FTO	Stannite structure The deposition time has a minor influence on the gap energy	This work

as an absorber in high-performance solar cells based on CCTS.

Author contributions Omar Ait Layachi: wrote the main manuscript text and prepared figures. All authors reviewed the manuscript.

Declarations

Competing interests The authors declare no competing interests.

References

- Murali B, Krupanidhi SB (2013) Facile synthesis of Cu₂CoSnS₄ nanoparticles exhibiting red-edge-effect: application in hybrid photonic devices. *J Appl Phys* 114:144312. <https://doi.org/10.1063/1.4825070>
- Green MA, Dunlop ED, Yoshita M, Kopidakis N, Bothe K, Siefert G, Hao X (2023) Solar cell efficiency tables (version 62). *Prog Photovolt* 31:651–663. <https://doi.org/10.1002/ppp.3726>
- Hammami H, Marzougui M, Oueslati H, Rabeh MB, Kanzari M (2021) Synthesis, growth and characterization of Cu₂CoSnS₄ thin films via thermal evaporation method. *Optik* 227:166054. <https://doi.org/10.1016/j.ijleo.2020.166054>
- Zaberca O, Gillorin A, Durand B, Chane-Ching JY (2011) A general route to the synthesis of surfactant-free, solvent-dispersible ternary and quaternary chalcogenide nanocrystals. *J Mater Chem* 21:6483. <https://doi.org/10.1039/c1jm10894h>
- Gillorin A, Balocchi A, Marie X, Dufour P, Chane-Ching JY (2011) Synthesis and optical properties of Cu₂CoSnS₄ colloidal quantum dots. *J Mater Chem* 21:5615. <https://doi.org/10.1039/c0jm03964k>
- Cui Y, Deng R, Wang G, Pan D (2012) A general strategy for synthesis of quaternary semiconductor Cu₂MnSnS₄ (M = Co²⁺, Fe²⁺, Ni²⁺, Mn²⁺) nanocrystals. *J Mater Chem* 22:23136. <https://doi.org/10.1039/c2jm33574c>
- Azmi S, Layachi OA, Ouadi ME, Khoumri EM, Moujib A, Brouzi AE, Nohair M, Pezzato L, Dabala M (2022) Growth of Cu₂ZnSnS₄ thin film absorber layer on transparent conductive oxides and molybdenum substrates by electrodeposition for photovoltaic application. *Optik* 250:168320. <https://doi.org/10.1016/j.ijleo.2021.168320>
- Wang T, Zhan Q, Cheng W (2019) Synthesis and characterization of Cu₂CoSnS₄ thin films prepared via radio-frequency (RF) magnetron sputtering. *J Mater Sci Mater Electron* 30:2285–2291. <https://doi.org/10.1007/s10854-018-0499-6>
- Moriya K, Tanaka K, Uchiki H (2007) Fabrication of Cu₂ZnSnS₄ thin-film solar cell prepared by pulsed laser deposition. *Jpn J Appl Phys* 46:5780–5781. <https://doi.org/10.1143/JJAP.46.5780>
- Ansari MZ, Khare N (2017) Effect of intrinsic strain on the optical band gap of single phase nanostructured Cu₂ZnSnS₄. *Mater Sci Semicond Process* 63:220–226. <https://doi.org/10.1016/j.mssp.2017.02.011>
- Krishnaiah M, Bhargava P, Mallick S (2015) Low-temperature synthesis of Cu₂CoSnS₄ nanoparticles by thermal decomposition of metal precursors and the study of its structural, optical and electrical properties for photovoltaic applications. *RSC Adv* 5:96928–96933. <https://doi.org/10.1039/C5RA18679J>
- Ansari MZ, Khare N (2014) Structural and optical properties of CZTS thin films deposited by ultrasonically assisted chemical vapour deposition. *J Phys D Appl Phys* 47:185101. <https://doi.org/10.1088/0022-3727/47/18/185101>
- Maldar PS, Gaikwad MA, Mane AA, Nikam SS, Desai SP, Giri SD, Sarkar A, Moholkar AV (2017) Fabrication of Cu₂CoSnS₄ thin films by a facile spray pyrolysis for photovoltaic application. *Sol Energy* 158:89–99. <https://doi.org/10.1016/j.solener.2017.09.036>
- Maldar PS, Mane AA, Nikam SS, Giri SD, Sarkar A, Moholkar AV (2017) Temperature dependent properties of spray deposited Cu₂CoSnS₄ (CCTS) thin films. *J Mater Sci Mater Electron* 28:18891–18896. <https://doi.org/10.1007/s10854-017-7842-1>
- López-Vergara F, Galdámez A, Manríquez V, González G (2015) Crystal structure and Raman scattering characterization of Cu₂Fe_{1-x}Co_xSnS₄ chalcogenide compounds. *Solid State Sci* 49:54–60. <https://doi.org/10.1016/j.solidstatesciences.2015.09.010>
- Zhang X, Bao N, Lin B, Gupta A (2013) Colloidal synthesis of wurtzite Cu₂CoSnS₄ nanocrystals and the photoresponse of spray-deposited thin films. *Nanotechnology* 24:105706. <https://doi.org/10.1088/0957-4484/24/10/105706>
- Oubakalla M, Beraich M, Taibi M, Majdoubi H, Guenbour A, Bellaouchou A, Addou M, Bentiss F, Zarrouk A, Fahoume M (2022) Effects of co-electrodeposition potential on the physicochemical properties of Cu₂CoSnS₄ thin films enriched by a theoretical calculation. *Int J Light Electron Opt*. <https://doi.org/10.1016/j.ijleo.2022.168886>
- Beraich M, Taibi M, Guenbour A, Zarrouk A, Boudalia M, Bellaouchou A, Tabyaoui M, Sekkat Z, Fahoume M (2019) Synthesis and characterization of Cu₂CoSnS₄ thin film via electrodeposition technique for solar cells. *J Mater Sci Mater Electron* 30:12487–12492. <https://doi.org/10.1007/s10854-019-01608-2>
- El Ouardi M, Ait Layachi O, Amaterz E, El Idrissi A, Taoufyq A, Bakiz B, Benhachemi A, Arab M, BaQais A, Ahsaine HA (2023) Photo-electrochemical degradation of rhodamine B using electrodeposited Mn₃(PO₄)₂·3H₂O thin films. *J Photochem Photobiol Chem* 444:115011. <https://doi.org/10.1016/j.jphotochem.2023.115011>
- Azmi S, Moujib A, Layachi OA, Matei E, Galca AC, Zaki MY, Secu M, Rusu MI, Grigorescu CEA, Khoumri EM (2020) Towards phase pure kesterite Cu₂ZnSnS₄ absorber layers growth via single step free sulfurization electrodeposition under a fix applied potential on Mo substrate. *J Alloy Compd* 842:155821. <https://doi.org/10.1016/j.jallcom.2020.155821>
- Bryden KJ, Ying JY (1998) Pulsed electrodeposition synthesis and hydrogen absorption properties of nanostructured palladium-iron alloy films. *J Electrochem Soc* 145:3339–3346. <https://doi.org/10.1149/1.1838809>
- Gurav KV, Yun JH, Pawar SM, Shin SW, Suryawanshi MP, Kim YK, Agawane GL, Patil PS, Kim JH (2013) Pulsed electrodeposited CZTS thin films: effect of duty cycle. *Mater Lett* 108:316–319. <https://doi.org/10.1016/j.matlet.2013.06.062>
- Termsaithong P, Munprom R, Shah A, Rodchanarowan A (2018) Pulsed current co-electrodeposition of kesterite Cu₂ZnSnS₄ absorber material on fluorinated tin oxide (FTO) glass substrate. *Surf Coat Technol* 350:807–812. <https://doi.org/10.1016/j.surfcoat.2018.04.045>
- Gurav KV, Kim YK, Shin SW, Suryawanshi MP, Tarwal NL, Ghorpade UV, Pawar SM, Vanalakar SA, Kim IY, Yun JH, Patil PS, Kim JH (2015) Pulsed electrodeposition of Cu₂ZnSnS₄ thin films: effect of pulse potentials. *Appl Surf Sci* 334:192–196. <https://doi.org/10.1016/j.apsusc.2014.09.079>
- Jeon M, Shimizu T, Shingubara S (2011) Cu₂ZnSnS₄ thin films and nanowires prepared by different single-step electrodeposition method in quaternary electrolyte. *Mater Lett* 65:2364–2367. <https://doi.org/10.1016/j.matlet.2011.05.003>
- Azmi S, Nohair M, Khoumri EM, El Marrakchi M, Dabala M (2018) Effect of the complexing agents on the properties of electrodeposited CZTS thin films. 7th international conference on renewable energy research and Applications, Paris, France. <https://doi.org/10.1109/ICRERA.2018.8566894>
- Boudouma A, Ait Layachi O, Hrir H, Khoumri E (2023) A one-step electrodeposition method was used to produce monoclinic Cu₂SnS₃ thin films for the development of solar cells. *J Mater Sci Mater Electron* 34:1903. <https://doi.org/10.1007/s10854-023-11390-x>

28. Layachi OA, Azmi S, Moujib A, El Khomri MN (2023) Investigation of nucleation and growth mechanism of $\text{Cu}_2\text{ZnSnS}_4$ absorber layer electrodeposition on Indium Tin Oxide coated glass. *Thin Solid Films* 782:140019. <https://doi.org/10.1016/j.tsf.2023.140019>
29. Tsai H-W, Chen C-W, Thomas SR, Hsu C-H, Tsai W-C, Chen Y-Z, Wang Y-C, Wang ZM, Hong H-F, Chueh Y-L (2016) Facile growth of $\text{Cu}_2\text{ZnSnS}_4$ thin-film by one-step pulsed hybrid electro-phoretic and electroplating deposition. *Sci Rep* 6:19102. <https://doi.org/10.1038/srep19102>
30. Chang B-Y, Park S-M (2010) Electrochemical impedance spectroscopy. *Ann Rev Anal Chem* 3:207–229. <https://doi.org/10.1146/annurev.anchem.012809.102211>
31. Herrera Hernández H, Ruiz Reynoso AM, Trinidad González JC, González Morán CO, Miranda Hernández JG, Mandujano Ruiz A, Morales Hernández J, Orozco Cruz R (2020) Electrochemical impedance spectroscopy (EIS): a review study of basic aspects of the corrosion mechanism applied to steels. In: El-Azazy M, Min M, Annus P (eds) *Electrochemical impedance spectroscopy*. IntechOpen. <https://doi.org/10.5772/intechopen.94470>
32. Yuan Y, Luo G, Li N (2021) New in situ description of electrode-positing multiple nucleation processes under galvanostatic stimuli. *RSC Adv* 11:31526–31532. <https://doi.org/10.1039/D1RA04988G>
33. Ordine AP, Díaz SL, Margarit ICP, Barcia OE, Mattos OR (2006) Electrochemical study on Ni–P electrodeposition. *Electrochim Acta* 51:1480–1486. <https://doi.org/10.1016/j.electacta.2005.02.129>
34. Korjenic A, Raja KS (2019) Electrochemical stability of fluorine doped tin oxide (FTO) coating at different pH conditions. *J Electrochem Soc* 166:C169–C184. <https://doi.org/10.1149/2.0811906jes>
35. Hsu CH, Mansfeld F (2001) Technical Note: concerning the conversion of the constant phase element parameter Y_0 into a capacitance. *Corrosion* 57:747–748. <https://doi.org/10.5006/1.3280607>
36. Hirschorn B, Orazem ME, Tribollet B, Vivier V, Frateur I, Musiani M (2010) Determination of effective capacitance and film thickness from constant-phase-element parameters. *Electrochim Acta* 55:6218–6227. <https://doi.org/10.1016/j.electacta.2009.10.065>
37. Valahia L, Olteanu RM, Ion IA, Bucurică IV, Gurgu ID, Dulamă ST (2020) ITO and FTO coated glass characterization using SEM and AFM techniques. *Bull Transilv Univ Brasov Ser* 12(61):41–46
38. Ahmadi M, Guinel MJ-F (2013) Synthesis, characterization and understanding of the mechanisms of electroplating of nanocrystalline–amorphous nickel–tungsten alloys using in situ electrochemical impedance spectroscopy. *J Alloy Compd* 574:196–205. <https://doi.org/10.1016/j.jallcom.2013.04.033>
39. I. Fotsing Etude Par voltammétrie cyclique des conditions d'électrodeposition de phosphure de zinc pour des applications photovoltaïques, (n.d.) 145
40. Liu K, Wei A, Zhang W, Xiao Z, Zhao Y, Liu J (2019) Synthesis of vertically aligned CoS prismatic nanorods as counter electrodes for dye-sensitized solar cells. *J Mater Sci Mater Electron* 30:1541–1546. <https://doi.org/10.1007/s10854-018-0425-y>
41. Sheng X, Wang L, Chen G, Yang D (2011) Simple synthesis of flower-like In_2S_3 structures and their use as templates to prepare CuS particles. *J Nanomater* 2011:1–5. <https://doi.org/10.1155/2011/280216>
42. Oubakalla M, Beraich M, Taibi M, Majdoubi H, Aichi Y, Guenbour A, Bellaouchou A, Bentiss F, Zarrouk A, Fahoume M (2022) The choice of the copper concentration favoring the production of stoichiometric CuSbS_2 and $\text{Cu}_{12}\text{Sb}_4\text{S}_{13}$ thin films co-electrodeposited on FTO. *J Alloy Compd* 908:164618. <https://doi.org/10.1016/j.jallcom.2022.164618>
43. Chaki SH, Tailor JP, Deshpande MP (2014) Covellite CuS—single crystal growth by chemical vapour transport (CVT) technique and characterization. *Mater Sci Semicond Process* 27:577–585. <https://doi.org/10.1016/j.mssp.2014.07.038>
44. Harinipriya S, Cassian H, Sudha V (2021) Colloidal CCTS nanoparticle synthesis by solution method for solar photovoltaic applications. *J Market Res* 15:3558–3569. <https://doi.org/10.1016/j.jmrt.2021.09.134>
45. Tang Y-Q, Ge Z-H, Feng J (2017) Synthesis and thermoelectric properties of copper sulfides via solution phase methods and spark plasma sintering. *Crystals* 7:141. <https://doi.org/10.3390/cryst7050141>
46. Tlemçani TS, Benamar EB, Moursli FCE, Hajji F, Edfouf Z, Taibi M, Labrim H, Belhorma B, Aazou S, Schmerber G, Bouras K, Sekkat Z, Dinia A, Ulyashin A, Slaoui A, Abd-Lefdil M (2015) Deposition time effect on the physical properties of $\text{Cu}_2\text{ZnSnS}_4$ (CZTS) thin films obtained by electrodeposition route onto mocoated glass substrates. *Energy Procedia* 84:127–133. <https://doi.org/10.1016/j.egypro.2015.12.305>
47. Azmi S, Pezzato L, Sturaro M, Khomri EM, Martucci A, Dabalà M (2019) A green and low-cost synthetic approach based on deep eutectic choline-urea solvent toward synthesis of CZTS thin films. *Ionics* 25:2755–2761. <https://doi.org/10.1007/s11581-018-2719-8>
48. Beraich M, Taibi M, Guenbour A, Zarrouk A, Boudalia M, Bellaouchou A, Tabyaoui M, Mansouri S, Sekkat Z, Fahoume M (2019) Preparation and characterization of $\text{Cu}_2\text{CoSnS}_4$ thin films for solar cells via co-electrodeposition technique: effect of electrodeposition time. *Optik* 193:162996. <https://doi.org/10.1016/j.ijleo.2019.162996>
49. Oubakalla M, Beraich M, Taibi M, Majdoubi H, Guenbour A, Bellaouchou A, Addou M, Bentiss F, Zarrouk A, Fahoume M (2022) Effects of copper concentration on the properties of $\text{Cu}_2\text{CoSnS}_4$ thin films co-electrodeposited on the FTO substrate. *J Mater Sci Mater Electron* 33:12016–12025. <https://doi.org/10.1007/s10854-022-08162-4>
50. Ait Layachi O, Moujib A, El Khouja O, CatalinGalca A, Boudouma A, Azmi S, Nini M, Nohair M, Khomri E (2024) Electrodeposition mechanism of $\text{Cu}_2\text{CoSnS}_4$ thin films onto FTO-coated glass: effect of some additives. *J Electroanal Chem* 959:118177. <https://doi.org/10.1016/j.jelechem.2024.118177>

Publisher's Note Springer Nature remains neutral with regard to jurisdictional claims in published maps and institutional affiliations.

Springer Nature or its licensor (e.g. a society or other partner) holds exclusive rights to this article under a publishing agreement with the author(s) or other rightsholder(s); author self-archiving of the accepted manuscript version of this article is solely governed by the terms of such publishing agreement and applicable law.